PAPER Nr.: 14

Analysis of Helicopter Rotor–Fuselage Interaction

by

N. Bettschart and D. Gasser

ONERA – Office National d'Etudes et de Recherches Aérospatiales,

Châtillon, France

TWENTIETH EUROPEAN ROTORCRAFT FORUM

OCTOBER 4 - 7, 1994 AMSTERDAM

Printed by the Technical Highschool Haarlem

Analysis of Helicopter Rotor–Fuselage Interaction[1]

by

N. Bettschart and D. Gasser[2]

ONERA – Office National d'Etudes et de Recherches Aérospatiales,

Châtillon, France

Abstract

Theoretical and experimental studies on helicopter rotor–fuselage interactional aerodynamics are conducted at ONERA. Wind tunnel unsteady pressure measurements on the fuselage of a helicopter powered model (Dauphin, scaled at 1/7.7) are presented. The flow unsteadiness, mostly dominated by a frequency corresponding to the blade passage, is clearly apparent on these experimental results even for high advance ratios, when rotor–fuselage interaction is often supposed to be weaker than at low speed. Unsteady pressure signatures depend on the advance ratio variations if the transducer is located near the edge of the rotor wake, and on the rotor lift variations when the transducer is located inside the rotor wake "tube". A code based on the iterative coupling between a 3–D low order panel code with doublet and source distribution for the fuselage and a lifting line method for the rotor with a free wake modelization has been developed. An unsteady pressure computation module has been elaborated by writing explicitly the temporal potential variation. Comparisons between the experimental (unsteady pressure and instantaneous velocity field measurements) and analytical results are generally fairly good, showing that the computational method presented can predict complex and realistic helicopter configurations. Nevertheless the remaining discrepancies in the correlation show that the effort has to be pursued especially in the unsteady pressure computations as well as on the experimental determination of the rotor wake geometry.

1 Introduction

The development of efficient aerodynamic methods to compute the flowfield around helicopters, taking into account all their components (fuselage, rotors, lifting surfaces, etc..) is still facing a huge challenge.

On the one hand, the aerodynamic phenomena involved cover a large spectrum of problems such as unsteadiness, dynamic stall, blade vortex interaction, transonic flow and viscous effects. If some of these basic aerodynamics problems are well understood, and thus can be efficiently simulated, a robust technique which can be easily and accurately used when all these phenomena occur concurrently is still missing. Moreover the resolution of the complete Navier–Stokes equations with adequate grid density to obtain reliable results, which will be the final stage of rotorcraft CFD, is still suffering from a lack of computational performance (both memory and speed) and "know–how". Nevertheless, awaiting this future, designers, researchers and manufacturers need aerodynamic informations on the whole helicopter configuration. Consequently, assumptions have to be make when numerical methods dealing with complete helicopters are developed. These hypotheses can have a physical nature, for instance by neglecting the fluid viscosity, or by simplifying the configuration itself (calculations of helicopter aerodynamics without tail rotor). Anyway these approaches induce necessarily limitations, and a critical analysis of the numerical results is mandatory.

On the other hand, experimental studies on helicopter powered model in wind tunnels or flight tests require sophisticated equipment and the constitution of a useful data base for the validation of the methods is a very time consuming process and is therefore costly.

At the Aerodynamics Department of ONERA, experimental

1 This research was supported by the French Ministry of Defence (STPA "Service Technique des Programmes Aéronautiques" and DRET "Direction des Recherches et Etudes Techniques")

2 Ph. D. Student, ENSAM (Ecole Supérieure d'Arts et Métiers), Paris.

and theoretical studies on the helicopter rotor–fuselage aerodynamics have been undertaken in order to improve the understanding of the phenomena involved, as well as to develop and validate accurate and efficient computational methods.

A coupled method for helicopter rotor–fuselage configurations is under development by coupling two singularity codes. The first code, developed at ONERA, computes the fuselage by using a classical low order panel formulation with source and doublet distribution. The second one, simulating the rotor, was initially developed by Eurocopter France; it is a lifting line method with a prescribed vortex wake. A free rotor wake version of this code has been developed at ONERA. The iterative coupling between the fuselage and the rotor codes (either with or without a free rotor wake) is based on a quasi–steady approach and is achieved by an azimuthal marching technique. After the process convergence, a fuselage unsteady pressure computation is completed.

From the experimental point of view, tests have been conducted at the S2 Chalais–Meudon subsonic wind tunnel on a helicopter powered model. Unsteady pressure measurements on the fuselage surface of a realistic Dauphin model (scaled at 1/7.7) were performed for different advance ratios and simulated masses. The present tests complete the previous ones which consisted in the instantaneous measurement of the velocity field around the powered model by a Laser Doppler Velocimeter technique [1].

The theoretical methods used presently are briefly described, and then the main results of the unsteady pressure measurements are presented. Comparisons between theoretical and experimental results on the velocity field as well as on the fuselage unsteady pressure are shown and commented.

2 Description of the computational method (PEIRF code)

The PEIRF code (stands for "Programme d'Etude d'Interaction Rotor Fuselage") is based on an iterative coupling between two codes, one modeling the fuselage, the other one the rotor and its wake. The mathematical formulation of these two codes are briefly presented below, before describing the PEIRF code itself.

2.1 Fuselage code

A low order panel method (constant source and doublet) used for helicopter fuselage calculations has been developed at ONERA [2]. The fluid is assumed to be inviscid, incompressible and irrotational over the whole flowfield around the fuselage (potential flow) and is thus governed by the Laplace's equation:

$$\Delta \varphi = 0 \qquad (1)$$

where φ is the velocity potential ($\mathbf{V} = \nabla\varphi$). The solution φ of the linear equation (1) depends on the boundary conditions of the problem which include the two physical boundaries namely the fuselage surface and the "infinity" surface:

- a Neumann condition on the fuselage surface (zero normal velocity component):

$$\nabla\varphi \cdot \mathbf{n} = \frac{\partial\varphi}{\partial n} = 0 \qquad (2)$$

- the fluid is undisturbed far away from the fuselage:

$$\varphi \rightarrow \varphi_\infty \text{ at infinity} \qquad (3)$$

Using the linearity of the Laplace equation and Green's theorem, solution of (1) can be expressed, in an integral form, by the summation of elementary singularity (sources σ and doublets μ) distributions over the fuselage surface:

$$\varphi = \frac{1}{4\pi}\int_{\text{fuselage}} \left[\mu\mathbf{n}\cdot\nabla\left(\frac{1}{r}\right) - \sigma\left(\frac{1}{r}\right)\right] dS \qquad (4)$$

Nevertheless equation (4) does not represent a unique solution of (1), since an infinity of combinations of source and doublet distributions can be used. Considering a Dirichlet condition for the inner potential (i.e. inside the body) or, which is equivalent, that there is no flux across the solid boundary of the fuselage, the inner potential φ_{in} is then constant ($\frac{\partial\varphi_{in}}{\partial n} = 0$, see for instance [3]) and we can choose in particular

$$\varphi_{in} = \varphi_{\infty} \qquad (5)$$

Using this new boundary condition in equation (4), the perturbation potential $\varphi_p = \varphi_{in} - \varphi_{\infty}$ can be now expressed, at the surface of the fuselage by:

$$2\pi\,\varphi_p = \int_{\text{fuselage}} \left[\mu\,\mathbf{n}\cdot\nabla\left(\frac{1}{r}\right) - \sigma\left(\frac{1}{r}\right)\right] dS \qquad (6)$$

with an explicit form for the source term, using the slip condition (2):

$$-\sigma = \frac{\partial\varphi_{in}}{\partial n} = \frac{\partial\varphi_{\infty}}{\partial n} = \mathbf{n}\cdot\mathbf{V}_{\infty} \qquad (7)$$

The initial problem is now completely solvable and the knowledge of the singularity distributions, μ and σ, on the fuselage surface allows to compute the velocity on the fuselage surface:

$$\mathbf{V}_{\text{fuselage}} = \mathbf{V}_{\infty} + \sigma\mathbf{n} - \nabla_S\,\mu \qquad (8)$$

where ∇_S is the gradient operator on the fuselage surface ($\nabla_S\,\mu$ is the fuselage's tangential component of the perturbation velocity while $\sigma\mathbf{n} = -(\mathbf{n}\cdot\mathbf{V}_{\infty})\cdot\mathbf{n}$ is the normal component). Velocity at any point x around the fuselage is computed by differencing the potential:

$$\mathbf{V}(x) = \mathbf{V}_{\infty} + \frac{1}{4\pi}\nabla\left(\int_{\text{fuselage}} \left[\mu\,\mathbf{n}\cdot\nabla\left(\frac{1}{r}\right) - \sigma\left(\frac{1}{r}\right)\right] dS\right) \qquad (9)$$

Numerically, the fuselage surface is discretized with N *quadrilateral or triangular panels* and the singularities are supposed constant by panel. Equation (6) is discretized at each panel center and can be written as a linear system of N equations for N unknown values (doublet strength μ):

$$\sum_{j=1}^{N} A_{ij}\,\mu_j = b_i \qquad (10)$$

with $A_{ij} = 2\pi$

$$A_{ij} = -\int_{\Gamma_j} \frac{\partial}{\partial n_j}\left(\frac{1}{r_{ij}}\right) dS\,,\quad i \neq j$$

$$b_i = -\sum_{j=1}^{N} \mathbf{V}_{\infty}\cdot\mathbf{n}_j \int_{\Gamma_j} \frac{1}{r_{ij}}\,dS$$

Integration of A_{ij} and b_i are performed analytically using the Hess and Smith formulation [4]. The linear system (10) is then solved by classical techniques – LU decomposition or iterative methods – depending on the type of computer and the number N of fuselage panels.

2.2 Rotor code

The lifting line method used for the simulation of the rotor and its wake was initially developed by Eurocopter France (METAR code, "Modèle d'ETude de l'Aérodynamique du Rotor") [5]. The blades are replaced by lifting lines located on their mean chord and the actual continuous circulation distribution along the blade span is discretized by a step function (see figure 1). Despite these simplifications, METAR can take into account the real parameters of the blade such as

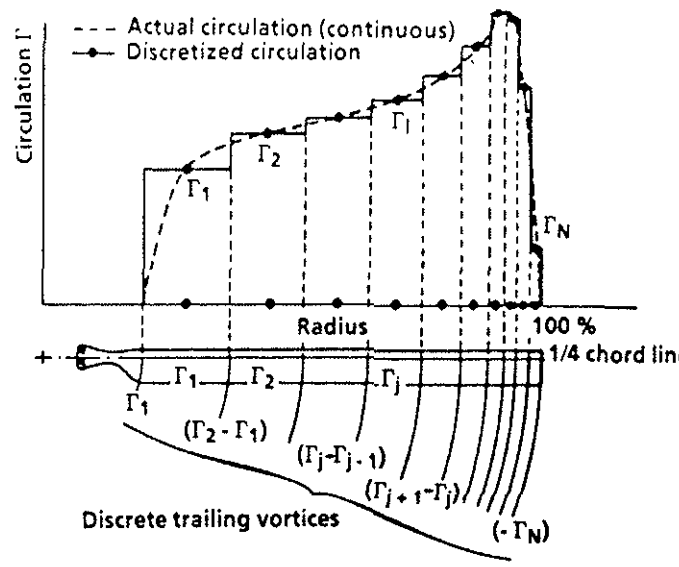

Fig. 1 – Rotor code – Blade discretization

evolutive chord, twist, anhedral, sweep, etc.. The rotor wake is represented by a lattice of longitudinal and radial linear vortex segments (figure 2) with a prescribed geometry. The vortex strength of a segment is related to the circulation of the lifting line at the time step (or azimuthal rotor position) and the span position where it was emitted. The rotor aerodynamic solution is carried out by an iterative process initialized by a mean Meijer-Drees induced velocity: the lift is obtained through 2-D experimental airfoil tables with the computed local angle of incidence and Mach number, and the circulation is derivated from the Joukowski law. The new velocity distribution induced by the rotor wake at the rotor collocation points is given by the Biot & Savart formula. Because the airfoil tables come from experimental results, real effects as dynamic stall, transonic flow, compressibility, are implicitly taken into account. The criterion of convergence of this process is based on the variation of the induced velocity distribution at the rotor control points between two successive iterations. Note that in this formulation, the Kelvin's theorem (conservation of the total angular momentum):

$$\frac{D\Gamma}{Dt} = 0 \qquad (11)$$

is implicitly verified since the vortex segments keep their strength while they are convected. The wake discretization covers only three rotor revolutions, which is sufficient for current applications.

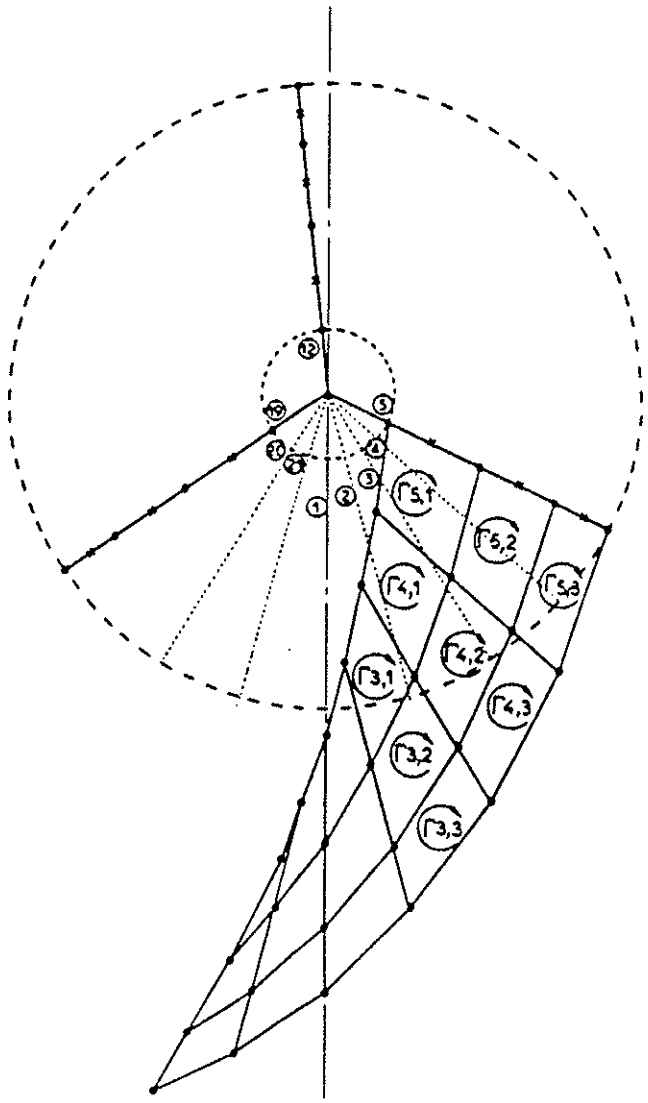

Fig. 2 – Rotor code – Rotor wake modelling

ONERA has developed a free wake version of the METAR code called MESIR ("Mise en Equilibre du Sillage Rotor"). The initial prescribed METAR rotor wake is distorted by taking into account the velocity induced by the rotor wake on itself [6]. For each rotor azimuth, the vortex segments are moved taking into account the velocity induced by the blades and the rotor wake itself instead of using a uniform inflow as is done in the METAR code. In this azimuthal marching technique, the strength of the vortex filaments are computed again at a frequency corresponding to the blade-to-blade interval. The criterion of convergence is based on the stability of the rotor wake geometry and for current applications, three rotor revolutions achieve a good convergence level.

2.3 Coupled method – PEIRF code

The iterative coupling procedure is based on a quasi-steady approach and is achieved by an azimuthal marching technique (see figure 3). Rotor and fuselage computations, considering these two elements as isolated, are used to initialize the process. Then two overlapped loops are started. For each azimuthal position of the rotor ψ_i, the most internal loop computes, at the rotor wake points, the velocity induced by the rotor and its wake $V_{rotor+wake}$ and by the fuselage $V_{fuselage}$. These rotor wake points are then moved and the new rotor wake geometry X_{i+1} is given by:

$$X_{i+1} = X(\psi + \Delta\psi) =$$

$$X_i + \left(V_{rotor+wake}(\psi) + V_{fuselage}(\psi) + V_\infty \right) \frac{\Delta\psi}{\Omega} \qquad (12)$$

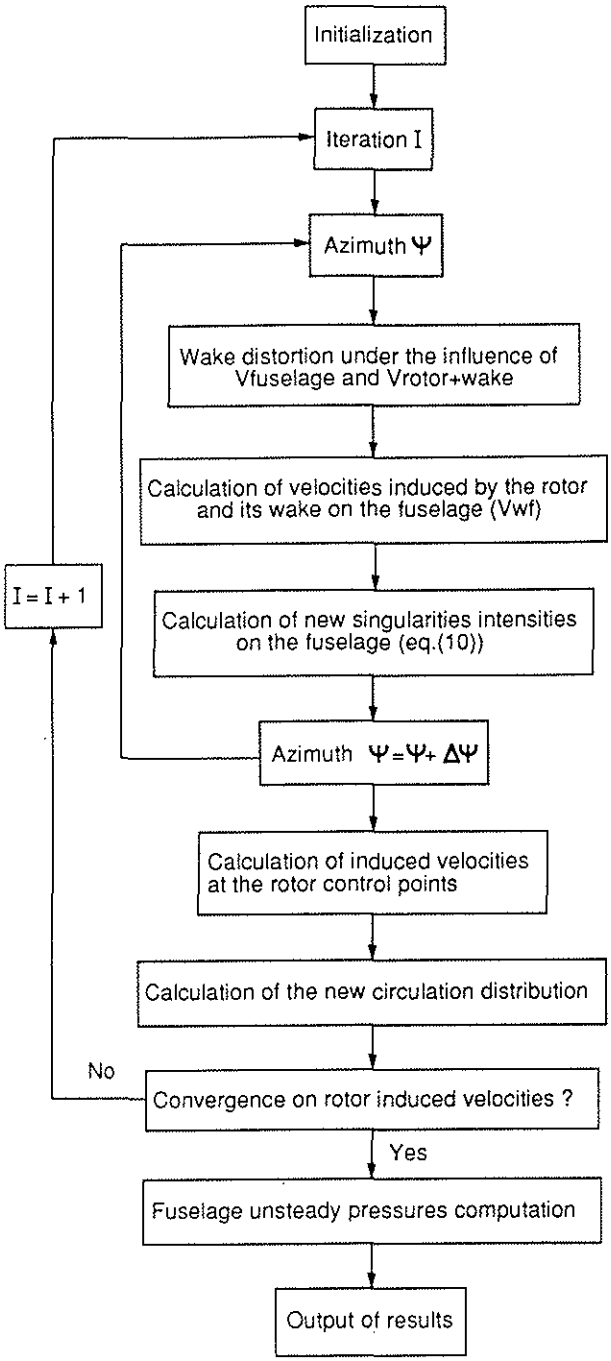

Fig. 3 PEIRF code – Flow chart

The fuselage is then immersed in this new rotor wake geometry and a fuselage calculation is performed in order to update the singularity strength, taking into account the velocity $\mathbf{V}_{wf}$ induced by the rotor wake on the fuselage. These velocities are computed, using the Biot and Savart formula, on the center of the fuselage panels. The new boundary condition (7) becomes:

$$-\sigma(\psi + \Delta\psi) = \mathbf{n} \cdot \left(\mathbf{V}_{\infty} + \mathbf{V}_{wf}(\psi + \Delta\psi) \right) \qquad (13)$$

Only the right hand side of the linear system (10) is modified (the Aij terms only depend on the fuselage geometry). The resolution of this new linear system is straightforward and very quick with a LU method because the inverse influence matrix is computed once, stored and the solution of (10) is therefore a simple matrix–vector product. If an iterative method is used, the resolution of (10) is not very time consuming too because the process can be initialized by the solution found at a previous iteration. Anyway, the resolution of equation (10) gives the doublet intensity distribution on the fuselage and the process is repeated for the new azimuthal position. It is not necessary to perform this inner loop for a whole rotor revolution, since the periodicity of this problem is limited to the blade–to–blade interval. The outer loop computes the new circulation due to the new rotor wake geometry. This is obtained, as in the METAR or MESIR codes, by the recursive process which links the induced velocities at the rotor control points and the rotor wake circulation via the airfoils tables, the local lift and the Joukowski law. Other code architectures have been tested, for instance inversion between the two loops (i.e. convergence first on the circulations for each azimuth), but the one presented here is the quicker and the more stable. Convergence of the algorithm is controlled looking at the evolution of the rotor wake geometry and of the induced velocities at the rotor control points.

Previous work has been already performed using this basic procedure [7]; however, significant improvements have been added to this original method.

First of all, the whole code architecture was rebuilt, some subroutines being completely rewritten, and validated on simple cases, in order to obtain a modular program. The present PEIRF version runs on various computer types (Cray YMP, Alliant, Sun, IRIS). This allows to have the same code for basics research (such as convergence tests, close interaction models,...) on simple rotor–fuselage interaction test cases with coarse rotor wake and fuselage discretizations, and for more realistic configurations where the fuselage can have up to several thousand panels.

Another important improvement of the method is the free rotor wake approach. The previous method coupled the fuselage code with the METAR code (prescribed rotor wake) while the PEIRF code couples the fuselage code with the MESIR code

(free wake method). It can be seen from equation (12) that the rotor wake geometry is deformed using the total local velocity.

Computations using singularity methods can be very time consuming when a good resolution is required, and thus the discretization is augmented. In particular, the induced velocities at the rotor wake points by the fuselage singularities can take more than 50 % of the total time. Several previous works (theoretical and experimental), [4], [7], [8] and [9], show that the fuselage effect becomes very weak, compared with the rotor wake effect, when the point considered is "far enough" from the fuselage. It was so natural, to save computational resources, to consider a far field and a near field in the computation of the induced velocity by the fuselage at the rotor wake points (equation (12)). The difficulty is to precise what "far enough" must be and thus to carry out an efficient and general algorithm. [4] presents the Hess and Smith formula considering a near field where the complete formulation is used and a far field where the quadrilateral constant source and doublet singularities are replaced by a point source and normal axis doublet located at the center of the panels. The second formulation (far field) is a very fast and accurate way to compute the velocity induced by a singularity panel when the distance between the point of interest and the panel center is more than 4-panel diagonals; in this case, the difference between the results given by the two formulations is less than 1 %. This far field formulation is of course wrong, even diverging, when the distance becomes small. Taking this above definition of "far", it can be see that very few rotor wake points are really "near" (i.e. at a distance less than 4-panel diagonals) of a panel center and when this occurs, this particular rotor wake point is near only of the few neighbouring panels and not of the whole panels composing the discretized fuselage. Therefore the following procedure has been developed for the computation of the velocity induced by the fuselage at the rotor points:

1. Computation of the induced velocity by each source and doublet panel at the rotor wake points, using the far field formulation. A cut-off is applied when the rotor wake is too close to a panel.
2. Computation of the distance r_{ij} between each couple of panel j and rotor wake point i. Comparison of this distance r_{ij} and the diagonal d_j of the panel j and determination of the couples (i,j) for which $\frac{r_{ij}}{d_j} \leq CRIT$, where CRIT is the criterion of transition "near field-far field" (usually set between 2 and 4).
3. For the (i,j) couples computed at the step 2, subtraction at the rotor wake point i of the contribution of the velocity induced by the panel j computed at step 1.
4. For the (i,j) couples computed at the step 2, computation, using the exact near field formula, of the contribution of panel j at the rotor point i.

This procedure seems quite complicated and time consuming because some contributions are computed three times. However, it should be noted that steps 1, 2 and 3 are very fast (they use only two overlapped loops) and that steps 3 and 4 are performed only for a little fraction of couples (i,j) depending of the criterion CRIT. For our current applications this fraction varies between 5 % and less than 1% of the total number of couples. This formulation allowed to decrease from a third up to a half of the computational time depending on the computational case and the type of computer used.

Finally, the last improvement presented here is the unsteady pressure computation on the fuselage. Because the PEIRF code is based on a quasi-steady approach, a specific algorithm has been developed. The unsteady pressure calculation occurs at the end of a PEIRF computation when the process is fully converged. The following paragraph presents the development of this calculation.

2.4 Fuselage unsteady pressure calculation

This calculation is based on the unsteady Bernoulli theorem:

$$\frac{\partial \varphi}{\partial t} + \frac{V^2}{2} + \frac{P}{\rho} = \text{constant on a streamline} \qquad (14)$$

Where φ is the potential, V the total velocity and P the static pressure.

Using (14) between the freestream and a point M on the fuselage surface, the unsteady pressure coefficient Cp_u can be defined as:

$$Cp_u(M,t) = 1 - \frac{V(M,t)^2}{V_\infty^2} - \frac{2}{V_\infty^2}\frac{\partial \varphi(M,t)}{\partial t} \qquad (15)$$

The total velocity V(M,t) is computed iteratively at each azimuth on the panel centers (see section 2.3). The main difficulty is then the calculation of the unsteady term $\frac{\partial \varphi(M,t)}{\partial t}$. The potential on the fuselage surface has three contributions:

$$\varphi(M,t) = \varphi_{rotor+wake}(M,t) + \varphi_\infty - \mu(M,t) \qquad (16)$$

where μ is the doublet intensity determined by equation (6). Note that $\mu(M,t)$ represents the difference between the fuselage inner and the outer potential. $\varphi_{rotor+wake}(M,t)$ is the potential induced by the rotor and its wake. Derivation of (16) gives:

$$\frac{\partial \varphi(M,t)}{\partial t} = \frac{\partial \varphi_{rotor+wake}(M,t)}{\partial t} - \frac{\partial \mu(M,t)}{\partial t} \qquad (17)$$

The time derivative of doublets μ is computed at each azimuth by finite difference, while the derivation of $\varphi_{rotor+wake}$ is analytically calculated by separating this potential into two potentials φ_{rotor} (blade potential) and φ_{wake}.

The rotor blades are modelized by lifting lines on which the circulation distribution is discretized by a step function (see section 2.2 and figure 1). To compute the potential induced by the blades φ_{rotor}, each segment of the lifting lines is replaced by a plane surfacic doublet of intensity $\mu_{rotor} = \Gamma_{rotor}$ (figure 4). Every point M on the fuselage is far enough from the blades to assimilate the surfacic doublet distribution to a doublet point located at the center of the blade panels. The time derivative of the potential induced by a doublet is therefore :

$$\frac{\partial \varphi_{rotor}(M,t)}{\partial t} =$$

$$\frac{S_d}{4\pi}\frac{\partial \mu_{rotor}}{\partial t}\frac{1}{r_0^2}\,\mathbf{i}_0 \cdot \mathbf{n}_0 + \frac{\mu_{rotor}}{4\pi} S_d \left(\frac{-2}{r_0^3}\frac{\partial r_0}{\partial t}\,\mathbf{i}_0 \cdot \mathbf{n}_0\right) \qquad (18)$$

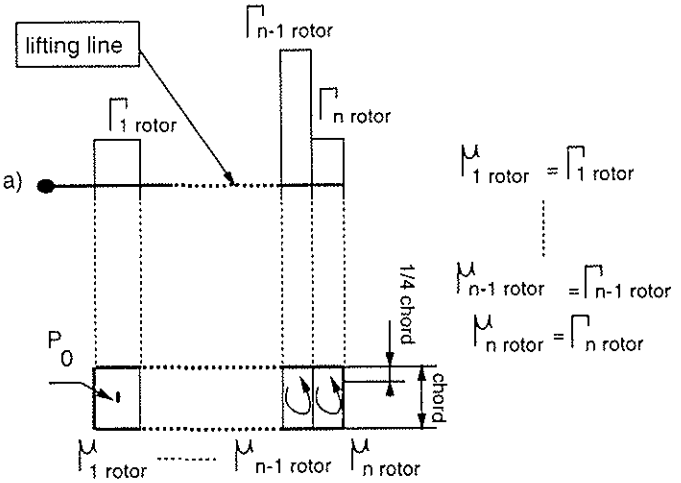

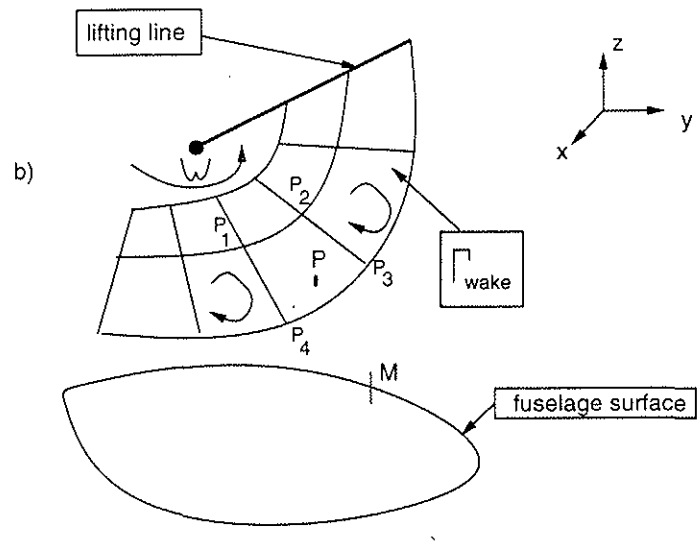

Fig. 4 – PEIRF code – Blade discretization for fuselage unsteady pressure computations

where $\mathbf{n}_0$ is the normal to blade panels, $r_0 = MP_0$ with P_0 center of the doublet, $\mathbf{i}_0 = \frac{\mathbf{MP}_0}{MP_0}$ and S_d is the doublet surface. The first term on the right hand side of equation (18) is proportional to the blade circulation changes and the second term corresponds to the blade velocity at point P_0.

The wake is simulated by a vortex sheet trailing from the lifting lines and constituted by a network of quadrilateral doublets (figures 2 and 4.b). The surfacic expression of the potential induced by each doublet can be transformed into a contour integral [10]:

$$\varphi_{wake}(M) = -\frac{\Gamma_{wake}}{4\pi}\iint_{S_d} \nabla_P\left(\frac{1}{r}\right) n_P \, ds = \frac{\Gamma_{wake}}{4\pi}\oint_C \frac{z \wedge r}{r\,(r+z\,.\,r)}\,dl \quad (19)$$

with r = MP, z is the vertical axis and C is the contour of a quadrilateral doublet $P_1P_2P_3P_4$ (figure 4.b). Since the intensity of each doublet Γ_{wake} is conserved with time (see section 2.2), the time derivative gives:

$$\frac{\partial \varphi_{wake}(M,t)}{\partial t} = \frac{\Gamma_{wake}}{4\pi}\sum_{i=1}^{4}\left[\int_{P_i}^{P_{i+1}} \dot{\left(\frac{A}{r}\right)}\cdot dl + \int_{P_i}^{P_{i+1}} \left(\frac{A}{r}\right)\cdot \dot{dl}\right] \quad (20)$$

where $\frac{A}{r} = \frac{z \wedge r}{r\,(r+z\cdot r)} = \frac{z \wedge u}{1+z\cdot u}\cdot\frac{1}{r}$ and $r = r\cdot u$

On the right hand side of equation (20), the first term takes into account the doublet convection effect and the second term the doublet distortion effect.

In order to simplify the calculations, the unit vector **u** is replaced by a mean direction u_0 between M and the middle of the segment P_iP_{i+1}. This allows to put the expression $A_0 = \frac{z \wedge u_0}{1+z\cdot u_0}$ out of the integrals.

After an analytical integration, we have :

$$\frac{\partial \varphi_{wake}(M,t)}{\partial t} = \frac{\Gamma_{wake}}{4\pi}\sum_{i=1}^{4}\left\{coef_1(i)\, V_{seg}\left(\frac{L_i}{L_i^2}\cdot A_0\right) + coef_2(i)\,[gradU]\left(\frac{L_i}{L_i}\cdot A_0\right)\right\} \quad (21)$$

with $coef_1(i) =$

$$\frac{L_i^4}{r_i^2L_i^2-(r_i\,L_i)^2}\left\{\arctan\frac{L_i^4+(r_i\,L_i)\,L_i^2}{r_i^2L_i^2-(r_i\,L_i)^2} - \arctan\frac{(r_i\,L_i)\,L_i^2}{r_i^2L_i^2-(r_i\,L_i)^2}\right\},$$

$$coef_2(i) = \ln\left(\frac{(r_i\,L_i)+\sqrt{(L_i^4+r_i^2L_i^2+2\,(r_i\,L_i)L_i^2+L_i^2}}{r_iL_i+(r_i\,L_i)}\right),$$

$\mathbf{L_i} = \mathbf{P_iP_{i+1}}$ and $\mathbf{r_i} = \mathbf{MP_i}$

V_{seg} stems from the time derivation of A and is the mean velocity of the segment $P_i\,P_{i+1}$ when [grad U] term is the velocity gradient along a segment P_iP_{i+1}: $[grad\ U] = \frac{(V_{P_{i+1}} - V_{P_i})}{L_i}\frac{L_i}{L_i}$.

Finally, the contribution of each doublet is added at each azimuth.

3 Experiment

Tests on an helicopter powered model have been performed in the ONERA S2 Chalais-Meudon wind tunnel. Unsteady pressure measurements on the fuselage have been done for different advance ratios ($0.1 \le \mu \le 0.3$) and simulated masses. The powered model was composed of a very detailed and realistic Dauphin fuselage (scaled at 1/7.7, about 1.5 meter long) and of a fully articulated hub with a four-bladed rotor. The rotor blades were rectangular with a constant OA209 (9% thick) airfoil of 0.05-meter constant chord, a -12° linear twist and a tip speed of 100 m/s for a diameter of 1.5 meter ($\Omega/2\pi$ = 21.2 Hz). The collective and cyclic pitch angles were controlled by three electrical actuators acting on a conventional swashplate. The flapping motion is measured and decomposed in Fourier series. Figure 5 shows the locations of the 44 unsteady pressure transducers (± 2 PSID measurement range). Each transducer was temperature compensated and calibrated individually before their installation in the fuselage shell.

Results presented in this paper were obtained on a full rotor revolution with a sampling frequency of 1.35 KHz (64 samples by revolution or $\Delta\psi$ = 5.6°). For a given flight test condition, the records were performed simultaneously on 24 transducers; two groups of 24 transducers were enough to

obtain a complete acquisition. Therefore 4 transducers allowed a crosschecking of the informations between the two groups. The transducer signals were recorded, for the 64 azimuthal positions, during 10 successive rotor revolutions, and an arithmetical average was then performed for each channel.

Figure 6 shows the mean static pressure coefficient C_p for transducers located on the upper longitudinal line for different advance ratios. For these cases, the mean pressure distribution is very similar as soon as the advance ratio is greater than μ = 0.2. For the lowest advance ratio (μ = 0.1), the pressure distribution and specially the pressure coefficient greater than unity, suggest severe rotor wake – fuselage interaction. The behaviour of these pressure distributions looks as if the rotor – fuselage interaction disappears or at least remains constant for advance ratios greater than μ = 0.15. Nevertheless the classical pressure coefficient C_p is not very suitable for helicopter analyses since it is difficult to separate clearly the effect of the advance ratio variations and the effect of the rotor wake interaction. A more appropriate pressure coefficient C_p^* is defined, normalized with the blade tip velocity which remains constant for all the tests, instead of using the freestream velocity (see for example [11]). Figure 7 presents the same data shown in figure 6 with the blade tip velocity normalization ($C_p^* = 100\ \mu^2\ C_p$). The decreasing interactional effect is not so strong as figure 6 would indicate.

Figure 8 shows the time history signals for transducers located on a upper longitudinal line for different advance ratios (μ = 0.1–0.15–0.2–0.3). At locations 4, 34 and 38 the unsteady responses are in phase, quite regular with a 4Ω quasi-sinusoidal shape and the advance ratio variations produce only amplitude changes. These behaviours can be interpreted as the blade passage effect. The transducers no. 11, 20 and 27 do not present the same regularity; for the low advance ratio ($\mu \leq 0.2$), the signals are also not very sensitive to the μ variations but for a high advance ratio (μ = 0.3), the unsteady responses become more chaotic. Transducers 11 and 20 present not only a 4Ω frequency response but also higher frequencies, when transducer 27 presents a complete disorganized response. These signatures are characteristic of a rotor wake-fuselage interaction. Nai-Pei Bi and G. Leishman [12] have described four characteristic unsteady pressure signatures on their unsteady pressure measurements for their helicopter powered model tests performed at the University of

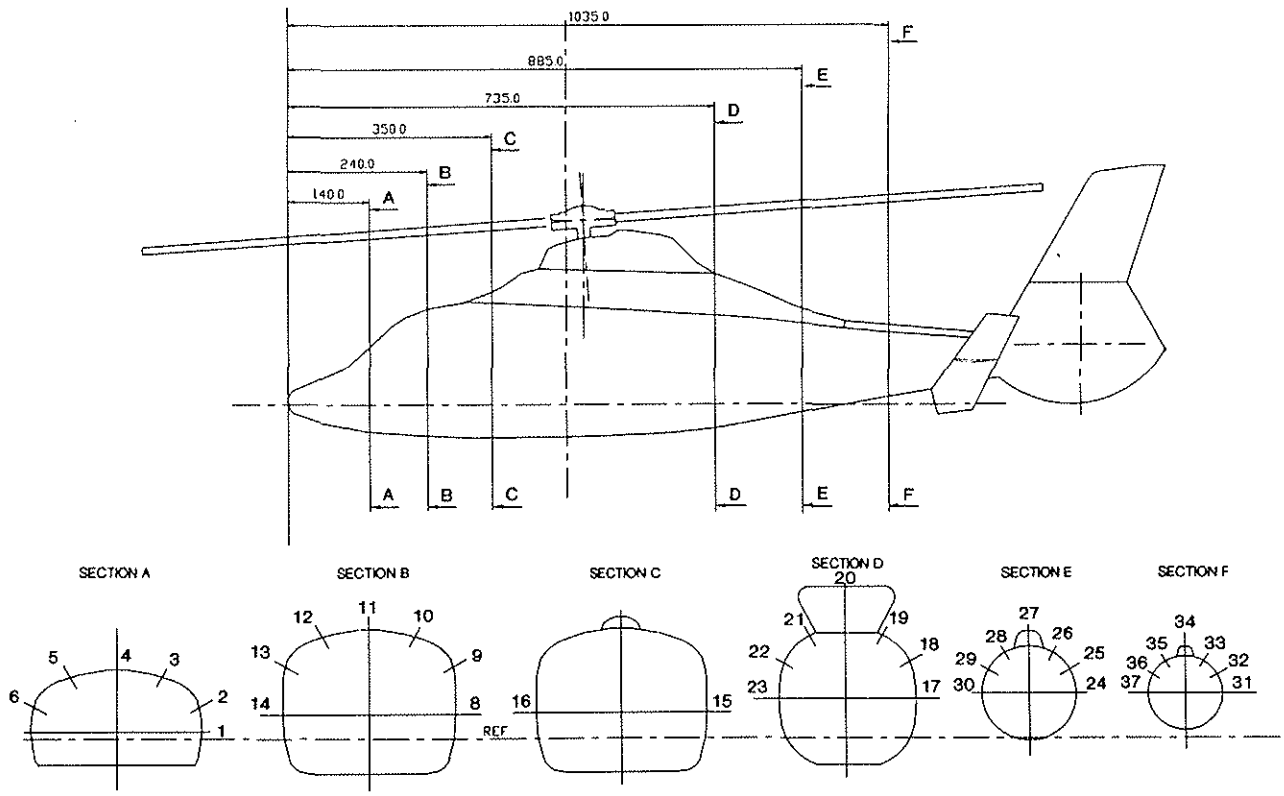

Fig. 5 – Fuselage unsteady pressure measurements – Transducer locations

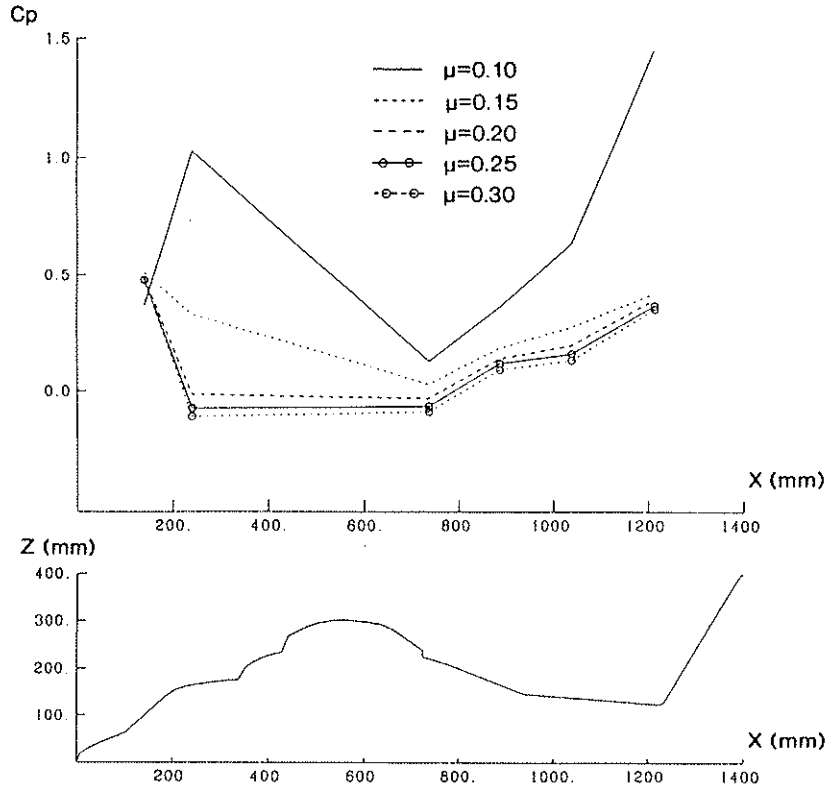

Fig. 6 – Fuselage unsteady pressure measurements – Mean static pressure coefficient Cp on the upper longitudinal line – CT/σ = 0.0725

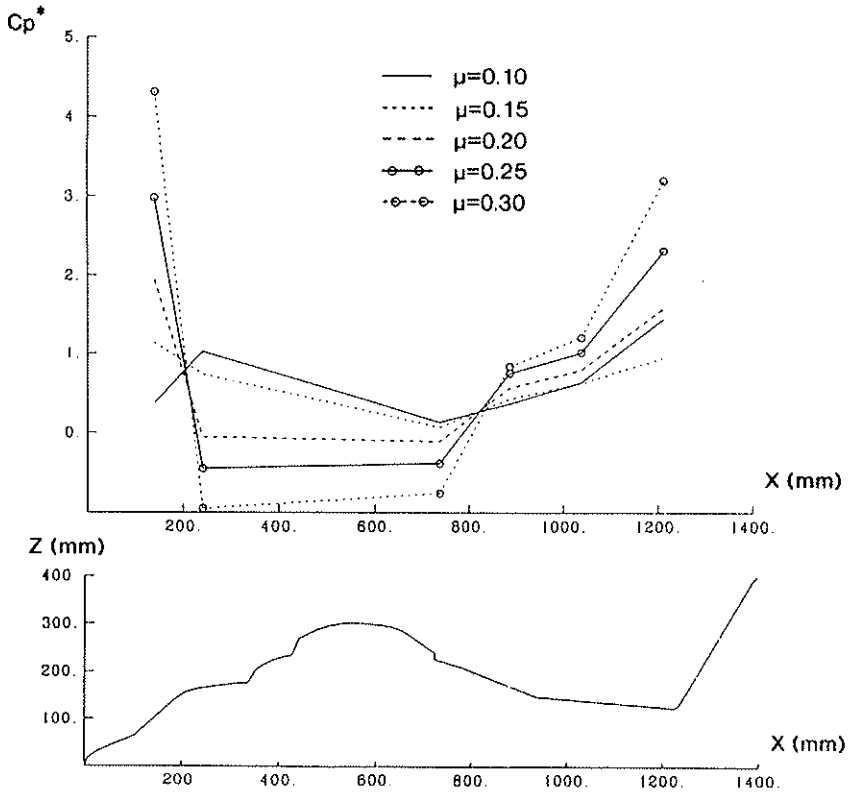

Fig. 7 –Fuselage unsteady pressure measurements – Mean static pressure coefficient C_p^* on the upper longitudinal line – CT/σ = 0.0725

Maryland. Their relevant analysis proposes a classification of these signatures: one is representative of the blade passage when the other three are typical of a direct or indirect rotor wake fuselage interaction (close wake-body interaction, rotor wake-body impingement and postwake impingement). In our Dauphin measurements, the blade passage effects are clearly apparent when the three types of rotor wake-fuselage interactions are not as recognizable as in the Maryland tests. This is probably due not only to the more complex Dauphin fuselage shape used in the ONERA tests, but also to the reduced number of runs (both advance ratios and simulated masses) performed at the S2 Chalais-Meudon wind tunnel.

Figure 9 presents the sensitivity of the unsteady response for rotor lift variations for a fixed advance ratio. For the locations outside the rotor wake (transducers 4 and 11), there are no changes in the signatures when variations of the rotor lift occur. On the other hand, for transducers 20, 27, 34 and 38 located inside the rotor wake, the fluctuations due to the blade passage effects are greater when the rotor lift is increased. This is a confirmation of the added energy throughout the rotor disc and in the rotor wake "tube".

Finally, in figures 8 and 9, some signals present also a strong 2Ω frequency (see for example figure 8, location 38 for μ = 0.1). This low frequency origin might be due to different blade characteristics but another origin could be low frequencies coming from the fuselage wake.

4 Comparison between calculation and experiment

Calculations were performed on the Dauphin powered model configurations.

4.1 Velocity field around the helicopter

The unsteady velocity field was measured around the Dauphin powered model using a three dimensional laser velocimeter (LDV) in two transversal planes located at x/R = 0 and x/R = 0.42 (figure 10) on the advancing side of the rotor disc [7]. The advance ratio was μ = 0.2 and the simulated mass corresponds to a rotor lift of C_T/σ = 0.0725.

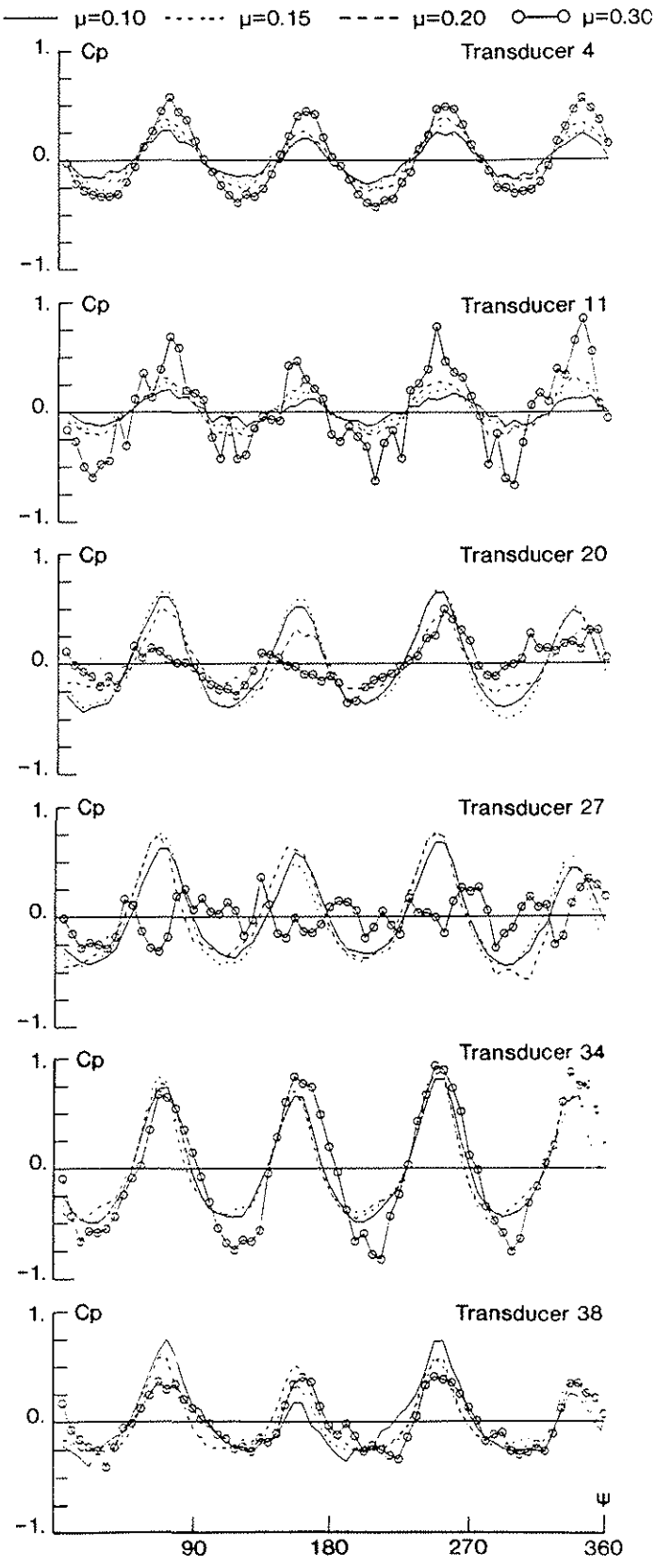

Fig. 8 – Fuselage unsteady pressure measurements – Time history on the upper longitudinal line for different advance ratios – C_T/σ = 0.0725

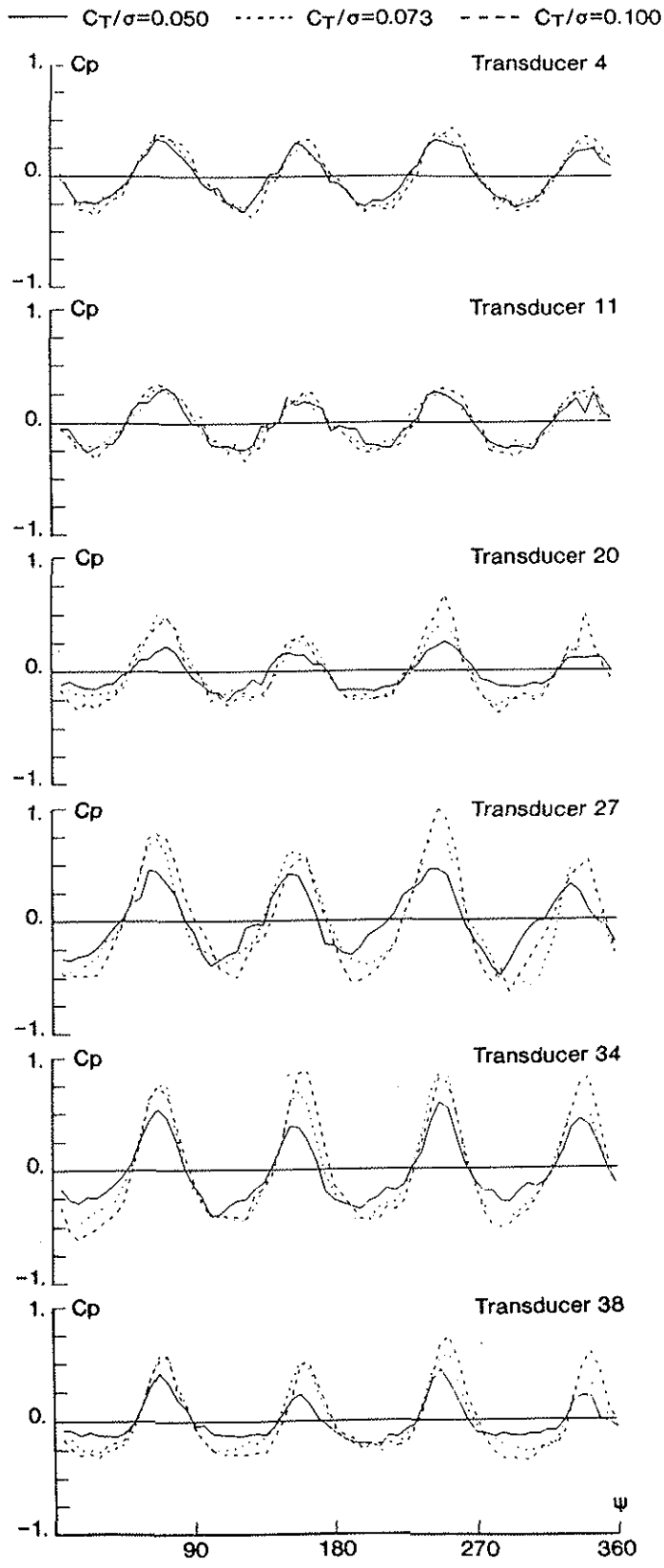

Fig. 9 – Fuselage unsteady pressure measurements – Time history on the upper longitudinal line for different rotor lift – μ = 0.2

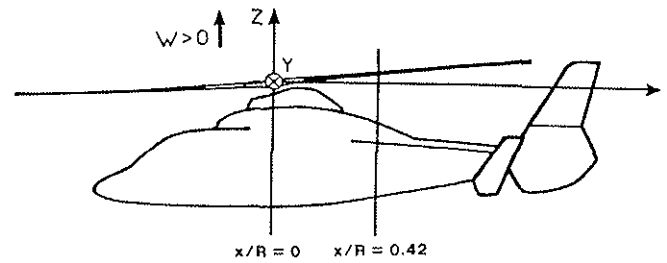

Fig. 10 – Configuration of the LDV measurements planes of the Dauphin powered model

Figures 11 and 12 show comparisons between two computational methods and experiment on the mean lateral velocity evolutions along the Y axis at different altitudes (z/R) for the two measurement planes. The first coupled rotor–fuselage computation is performed with the previous numerical method (METAR model for the rotor wake) when the second one is performed with the PEIRF code (MESIR free wake model for the rotor wake). The free wake model improves the comparison with experiment, in particular, for the more downstream plane, the velocity gradients, due to the mean effect of the tip vortices are quite well predicted by the PEIRF code. The free wake approach (PEIRF code) gives *certainly a better rotor wake geometry than the prescribed rotor* wake method. Near the fuselage (Y/R→0), the differences between free wake and prescribed wake models are visible only in the more downstream measurement plane (x/R = 0.42). The lack of experimental points in this region does not allow to draw further conclusions. Moreover, viscous effects, which are not accounted for by the potential code can also have a preponderant influence for these points located in the vicinity of the fuselage.

Instantaneous velocities (lateral and vertical component) are presented in figure 13 for points located in the more upstream plane, near the blade tip. Azimuthal evolutions of vertical and lateral instantaneous velocities (amplitudes and phases) are well predicted by the PEIRF code. The computational impulsiveness of the vertical component, characteristic of the blade passage effect, matches quite successfully the experimental result (see figure 13, y/R = 0.96).

4.2 Pressures on the fuselage surface

This paragraph presents the comparisons between computation and experiment for a test configuration described in section 3 (μ = 0.1, C_T/σ = 0.0725).

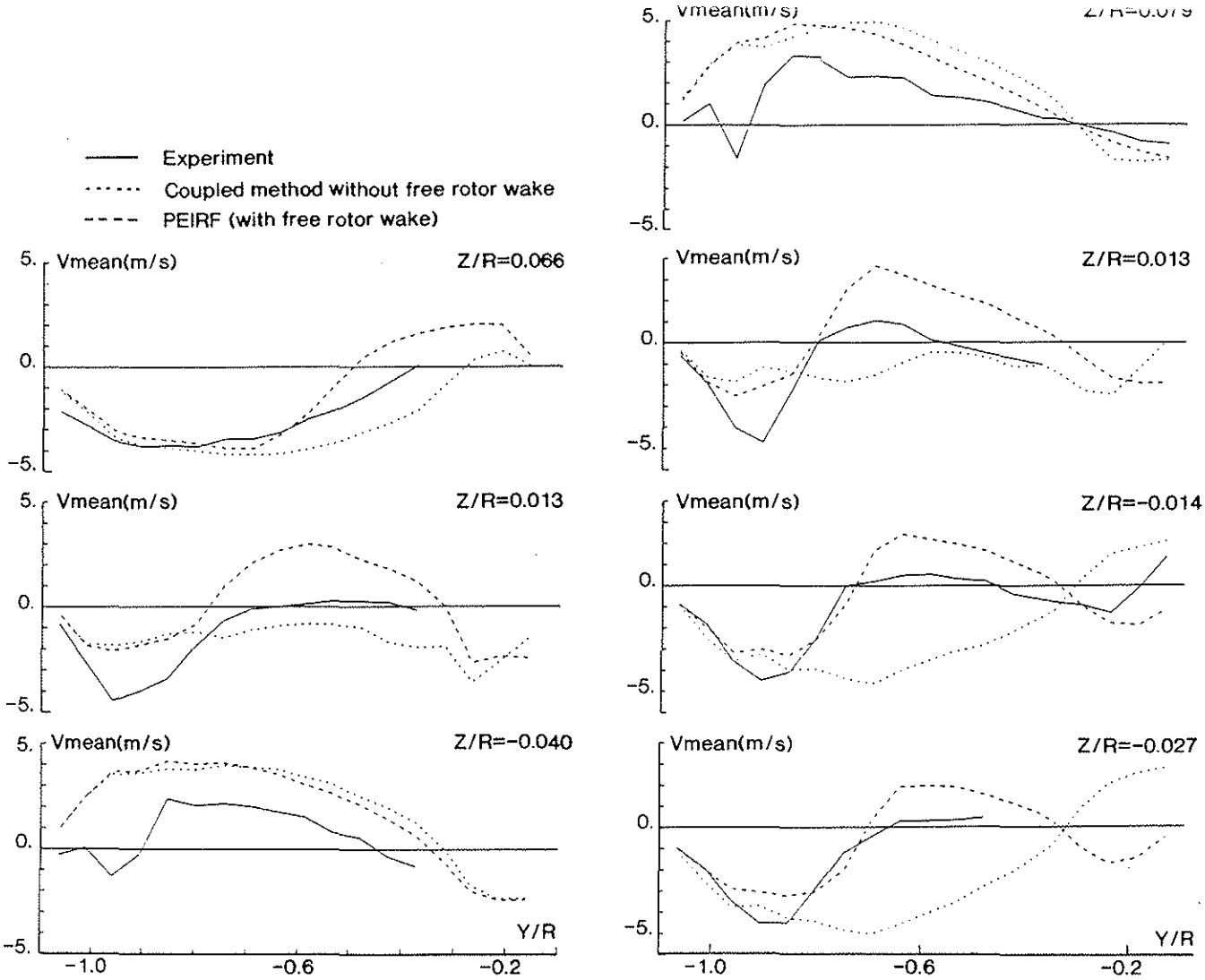

Fig. 11 Mean lateral velocities – x/R = 0

Fig. 12 Mean lateral velocities – x/R = 0.42

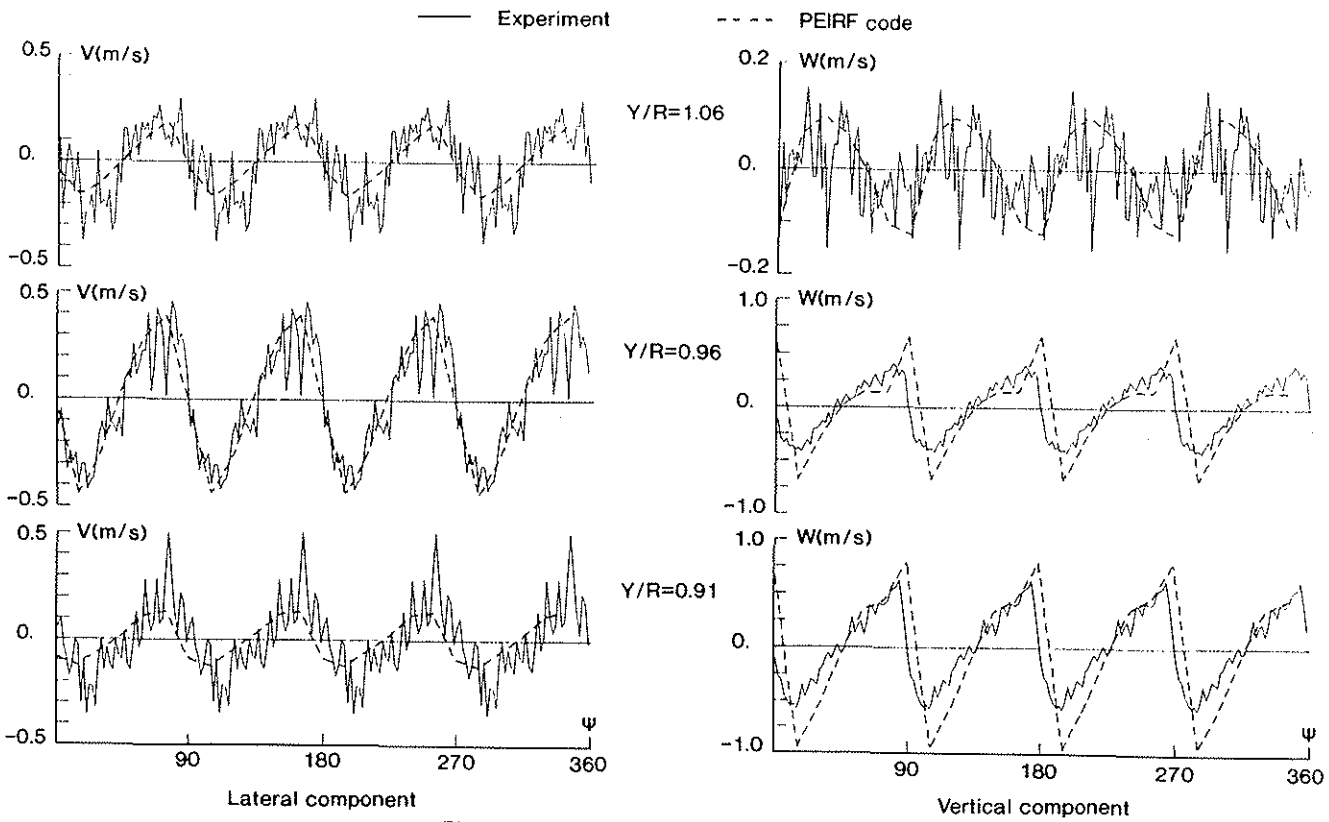

Fig. 13 Instantaneous velocities – x/R =0 – z/R = 0.04

Figure 14 shows the unsteady pressure coefficient evolution for different sensors located on the Dauphin fuselage top line. The quasi-steady computation only takes into account the local velocity to calculate the pressure coefficient (eq. (15) without the unsteady term $\partial\varphi/\partial t$). The other computation takes into account the unsteady term including the rotor+wake and the fuselage influence (equation (17)). Figure 15 shows the same sensors locations, with the influence of the blade effect only ($\partial\varphi_{rotor}/\partial t$, equation (18)) and of the total unsteady term ($\partial\varphi_{rotor}/\partial t + \partial\varphi_{wake}/\partial t$, equation (18) and equation (21)).

Figure 14 shows that the amplitude levels are mainly due to the unsteady term. Figure 15, shows that on sensor 4, the rotor effect is preponderant, because near the fuselage nose, the rotor wake is far and the main effect is due to blade passage. The calculation gives a regular sinusoidal signal, similar to experiment but with an underestimated amplitude and a shifted phase.

On sensor 11, the wake interacts the fuselage and is thus responsible for an irregular computed signal. The experimental signature is also characteristic of a wake-body interaction as discussed in section 3. On sensors 20, 27 and 34 downstream the hub, the wake effect is preponderant in comparison with the blade passage effect. The calculation gives an opposite phase on sensor 20 which is probably due to separated flow behind the fairings, which a potential code can not predict. On locations 27 and 34, where the fuselage has a smoother shape, the phase is then better predicted by calculation with an underestimated amplitude.

Figure 16 shows the pressure evolution on sensors located in a section near the empennages (section F). The wake effect is still preponderant. The unsteady wake effects computed by the PEIRF code improves the experimental correlation especially on the amplitude. This shows that the unsteadiness of the rotor wake must be taken into account in the computations. The shifted phase origin is not yet still completely understood; an hypothesis could be that the computed points do not coincide exactly with the real transducer locations. The relatively coarse azimuthal discretization ($\Delta\Psi$ = 15°) could be also responsible for this shifted phase.

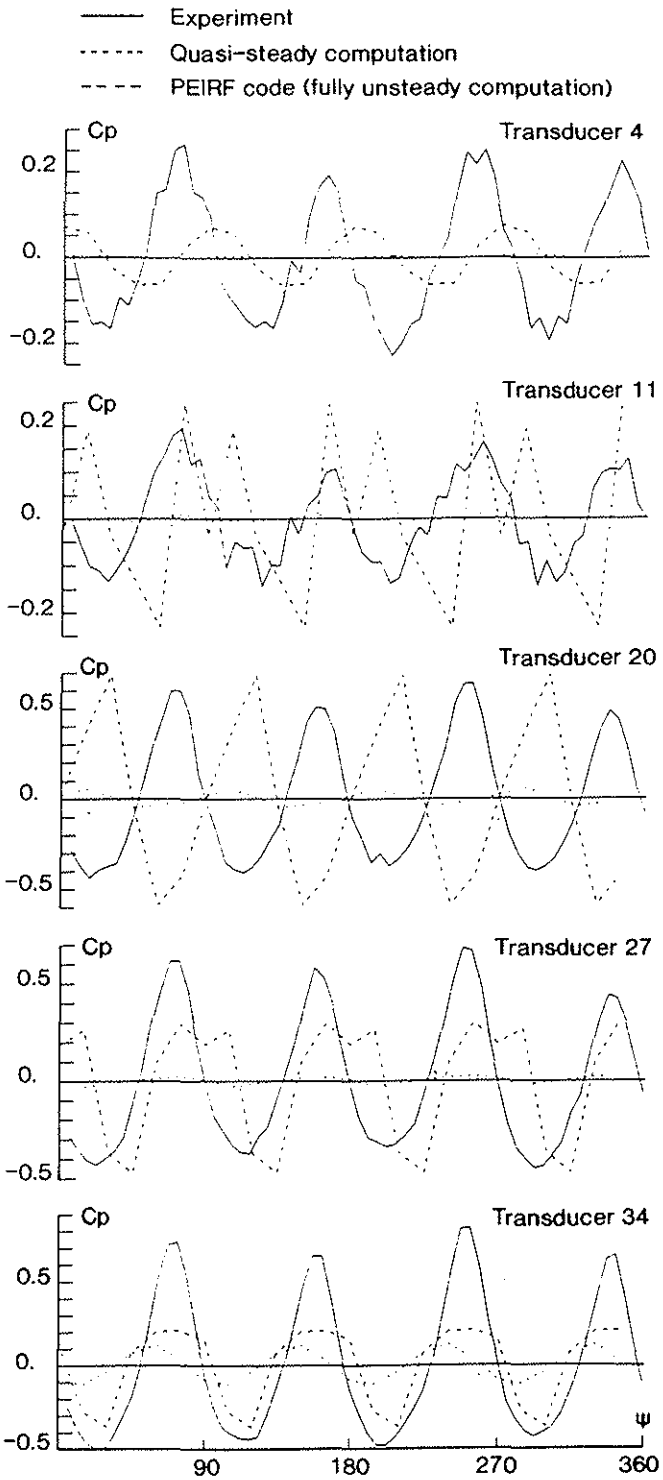

Fig. 14 – Unsteady pressure comparisons on the upper longitudinal line – $\mu = 0.1$ – $C_T/\sigma = 0.0725$

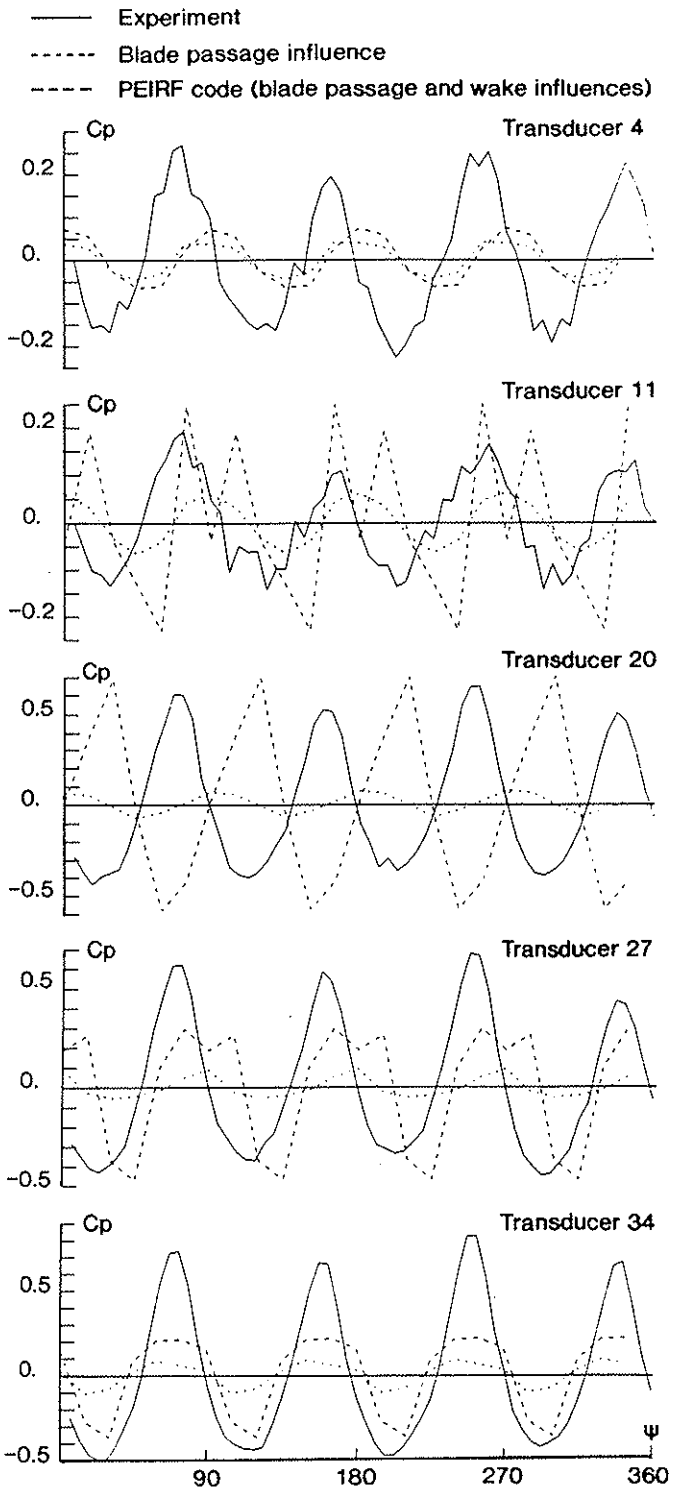

Fig. 15 – Unsteady pressure comparisons on the upper longitudinal line – μ = 0.1 – C_T/σ = 0.0725

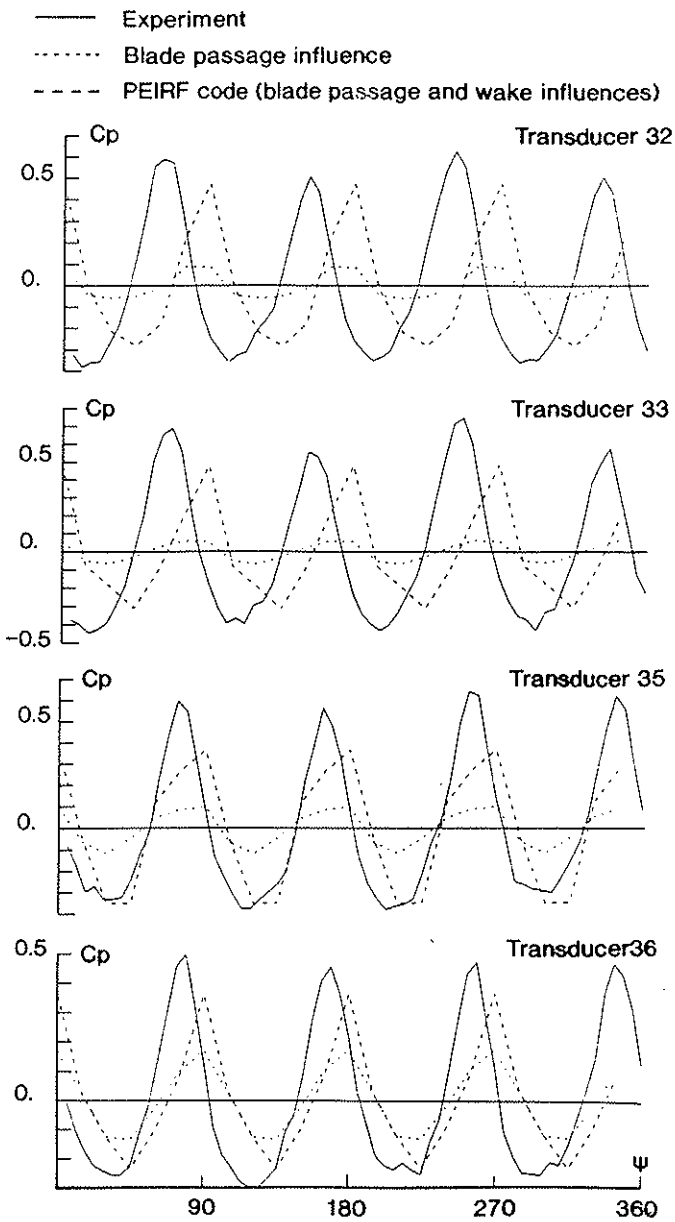

Fig. 16 – Unsteady pressure comparisons in section F – μ = 0.1 – C_T/σ = 0.0725

5 Conclusion

An experimental investigation has been performed on a Dauphin helicopter powered model in the S2 Chalais-Meudon wind tunnel. Unsteady and mean static pressure measurements on 44 locations on the fuselage have been achieved for different flight configurations. Mean static pressure coefficients greater than unity are observed on the fuselage surface meaning that energy is added by the rotor to the flow. The unsteady results show that the dominant frequency is linked to the blade passage effects; nevertheless when severe rotor wake-fuselage interactions occur, higher frequencies can also be present in the unsteady response. The unsteady pressure fluctuations are of the same magnitude or even can be greater than the mean value showing that unsteady effects must be taken into account in the numerical models. Two types of signature are clearly visible: one is characteristic of the blade passage effects, while the other one is dominated by rotor wake-fuselage interaction. The fuselage unsteady pressure signatures are sensitive to the rotor lift as well as to the advance ratio variations. Rotor lift variations change the fluctuation amplitudes, especially for the transducers located inside the rotor wake tube. Advance ratio variations affect in a highly nonlinear way the transducer responses, since at an advance ratio variation induces a variation of the rotor wake geometry and thus the locations of the rotor wake-fuselage interactions can move very quickly on the fuselage. Thus some transducers can have radical different responses with minor changes of the advance ratio. Consequently, the rotor wake geometry and the vortex filaments strength have to be carefully computed for accurate unsteady pressure computations.

A singularity method has been developed in order to predict the flow field around and on the helicopter fuselages. This quasi-steady method can handle realistic and complex configurations with little pre-processing efforts (the code only needs the geometry, the dynamic motions, the blade airfoil tables and a surfacic mesh for the fuselage). A module has been added in order to compute the explicit unsteady term in the Bernoulli equation and thus to evaluate the fuselage unsteady pressures. An efficient algorithm for the computation of the fuselage induced velocities at the rotor wake points has been developed and validated. Based on the consideration of a far field and a near field, this algorithm has allowed to save between a third and a half of the computational time.

Correlation between experimental and computed results show that even with the extreme complexity of the flowfield around helicopter, potential theory and singularity methods have a large range of applications. Nevertheless, separated flow regions and close rotor wake interactions with the fuselage are still areas for future works. The coupled method with a free wake computation (PEIRF code) improves the comparisons on the experimental mean velocities, even if some discrepancies are still present. Correlations on the fuselage unsteady pressures show that quasi-steady computations are not sufficient and that the unsteady terms have to be evaluated.

Future developments on the PEIRF code will include a fuselage boundary layer computations in order to have informations on the separated flow regions with and without the influence of the rotor wake. A spatiotemporal local time step when severe rotor wake-fuselage interactions occur is presently under development; this procedure which increases locally both the wake and the fuselage discretization will improve the convergence and the precision of the code.

Finally, additional experimental investigation on the Dauphin powered model will be carried out, particularly in order to have a better knowledge of the rotor wake geometry.

Acknowledgements

The authors wish to thank Eurocopter France for the technical support and especially the lending of the rotor blades.

References

[1] N. Bettschart, R. Hanotel, D. Ilbas, A. Desopper. *Experimental and Theoretical Studies of Helicopter Rotor Fuselage Interaction*. 17th European Rotorcraft Forum, University Berlin, Germany, September 1991.

[2] J. Ryan, G. Falempin, T.H. Le. *Rotor Plane Velocities Induced by a Helicopter Fuselage*. 2nd International Conference on Basic Research, College Park, Maryland, 16-18 February 1988.

[3] H. Lamb. *Hydrodynamics*. Dover Publication Inc. New York 1945.

[4] J. Katz, A. Plotkin. *Low speed Aerodynamics*. McGraw-Hill Inc., Series in Acronautical and Aerospace Engineering, New York, 1991.

[5] A. Dehondt, F. Toulmay. *Influence of Fuselage on Rotor Inflow Performance and Trim.* 15th European Rotorcraft Forum, Amsterdam, September 1989.

[6] B. Michéa, A. Desopper, M. Costes. *Aerodynamic rotor loads prediction method with free wake for low speed descent fights.* 18th European Rotorcraft Forum, Avignon, France. September 1992.

[7] N. Bettschart, A. Desopper, R. Hanotel, R. Larguier. *Experimental and Theoretical Studies of Helicopter Rotor Fuselage Interaction.* 18th ICAS Congress, Beijing, China, September 1992

[8] A. Bagai, J.G. Leishman. *Experimental Study of Rotor Wake/Body Interactions in Hover.* Journal of the American Helicopter Society, October 1992.

[9] J.D. Berry, S.L. Althoff. *Inflow Velocity Perturbations Due to the Presence of a Fully Interactive Wake.* 46th American Helicopter Society Annual Forum, May 1990, Washington DC.

[10] J.P. Guiraud. *Potentiel des Vitesses Créées par une Distribution Localisée de Tourbillon.* La Recherche Aérospatiale No. 6, Novembre–Décembre 1978, pp 365–366.

[11] A.G. Brand, H.M. McMahon, N.M. Komerath. *Surface Pressure Measurements on a Body Subject to Vortex Wake Interaction.* AIAA Journal, Vol. 27, No. 5, May 1989.

[12] Nai–Pei Bi, J.G. Leishman. *Analysis of Unsteady Pressures Induced on a Body by a Rotor.* Journal of Aircraft, Vol. 28, No. 11, November 1991.